Pol. J. Environ. Stud. Vol. 31, No. 5 (2022), 4229-4312
DOI: *10.15244/pjoes/148062* ONLINE PUBLICATION DATE: 2022-07-26

Original Research

The Variability of Net Primary Productivity and Its Response to Climatic Changes Based on the Methods of Spatiotemporal Decomposition in the Yellow River Basin, China

Biao Wang[1], Ruipeng Sun[1], Yongpeng Deng[1], Hongfen Zhu[1,2]*, Meiting Hou[3]

[1]College of Resources and Environment, Shanxi Agricultural University, Taigu, Shanxi 030801, China
[2]National Experimental Teaching Demonstration Center for Agricultural Resources and Environment, Shanxi Agricultural University, Taigu, Shanxi, 030801, China
[3]China Meteorological Administration (CMA) Training Centre, Beijing, 100081, China

Received: 24 November 2021
Accepted: 5 April 2022

Abstract

The fragile ecosystem in the Yellow River Basin (YRB) is sensitive to climatic changes, and previous studies have mainly focused on exploring the spatiotemporal relationship between vegetation growth and climatic change based on their spatially or temporally averaged values. However, few studies unraveled the effect of climatic changes on vegetation growth from both spatial and temporal variations separately. In the study, empirical orthogonal function (EOF), singular value decomposition (SVD), and trend analysis were used to detect the spatiotemporal variation of net primary productivity (NPP) over 2000-2019 and to analyze its response to climatic factors from spatial and temporal aspects, respectively, in the YRB. The results showed that the distribution of NPP decreased from southeast to northwest. The areas of NPP with significantly improved and degraded accounted for 80.41% and 1.3%, respectively. The NPP had greatly increased after 2012, particularly in the central region, but decreased in the eastern region. Precipitation was the dominant factor influencing NPP growth, especially in the arid and semi-arid regions. Additionally, the characterization of variability in farmland and forest land by EOF was better than SVD. This study provides insights into the relationship between vegetation growth and climatic changes at a watershed scale.

Keywords: vegetation dynamics, climatic changes, spatial and temporal dimensions, EOF, SVD

*e-mail: hongfzh@163.com

Introduction

Vegetation, as a component of the global terrestrial ecosystems, plays a critical role in global carbon balance, energy exchange, climate regulation and soil conservation [1]. The net primary productivity (NPP) is the difference between photosynthesis production and respiration consumption, and is an important variable for global carbon cycle and the feedback between terrestrial ecosystems and atmosphere [2]. It is an important indicator for earth system science research, climate change, and ecological environment assessment [3, 4]. With the effect of global warming, the suitable bioclimatic condition is more essential for vegetation growth, ecosystem functions and human lives [5, 6], and many studies analyzed the impacts of climatic changes on NPP variation, which is greatly sensitive to climatic changes [3, 7].

In general, precipitation and temperature are the main climatic factors affecting the variation of NPP. Some studies found that the annual precipitation had the widest impact on the NPP, particularly in the areas where precipitation was less abundant [8, 9]. Temperature is conducive to the growth of NPP in the Tibet Plateau because of the higher sensitivity in alpine vegetation, and solar radiation also have a positive impact on NPP in most parts of China [7]. The correlation and time-lag effects between NPP and climatic factors under vegetation types were detected, which might be related to geographical location and terrain factors [10, 11]. Furthermore, several studies analyzed the spatiotemporal changes of grassland NPP under climate scenario RCP2.6 and RCP8.5 by 2050 [12], evaluating the NPP in response to climatic changes in the future [1]. Thus, it is essential to investigate the relationships between NPP and climatic factors to better understand the driving mechanism of global climatic change on ecosystem functions.

Various methods were used to investigate the relationship between NPP and climatic factors. The Pearson's correlation coefficients were employed to assess the relationship between NPP and the extreme climate indices in coastal China from 1986 to 2015 [13]. The relationship between NPP and climate change in different vegetation zones in northwest China were assessed based on Ensemble Empirical Mode Decomposition (EEMD) detrending analysis [14]. Moreover, the threshold segmentation method was used to detect the NPP dynamics affected by both climate and ecological restoration projects in eight ecoregions and its driving mechanisms [15]. Obviously, the spatiotemporal changes of NPP in large area is the results of interactive effects of climate on both spatial and temporal variation. However, previous studies about the spatial effects of climate on NPP were mainly based on the temporally averaged values of NPP and climatic factors ignoring their temporal variation [14, 16], and studies about the temporal effects of climate on NPP were mainly based on their spatially averaged values ignoring their spatial variation [17, 18], which did not attempt to disentangle the spatial and temporal effects of climate on NPP.

The empirical orthogonal function (EOF) and singular value decomposition (SVD) analysis have the advantages to analyze the geographic variables with spatial and temporal variation for decomposing them into a set of spatial patterns of variability and corresponding time series. The decomposed spatial modes could exhibit spatial structure of geographic variables and are helpful for understanding their physical meanings, which is controlled by the variability of spatial variables, and the decomposed temporal series could represent detail information of inter-annual variations [19, 20]. Considering the entangled spatiotemporal effects of climatic factors on the spatial and temporal variation of NPP, the methods of EOF and SVD might be better to characterize the spatiotemporal variability of variables. For example, the EOF analysis was employed to detect temporal patterns and spatial variability of Normalized Difference Vegetation Index (NDVI) after typhoons in the mountainous watershed [21]. The spatiotemporal variability of NDVI associate with deforestation was analyzed in four zones in southeastern Peru by using EOF [22]. Some researchers applied EOF and SVD analysis to identified the main modes of variability of NDVI and their relationships with precipitation and temperature [23], and detected the temporal lags and the interactions between climatic factors at some ecosystems [19]. The EOF and SVD analysis were also applied to investigate the coupled effects of the dynamics of leaf area index (LAI) and climatic variabilities at a watershed scale [24]. However, the capabilities of EOF and SVD on separating and explaining the spatial and temporal variation of NPP were not compared. Therefore, this study attempts to analyze the dynamics of NPP and its response to climatic change from both temporal and spatial dimensions by both methods of EOF and SVD, and to explore the differences between the two methods on figuring out the spatial and temporal effect of climate on NPP in the Yellow River Basin (YRB) of China.

The YRB is the second longest river in China, spanning arid, semi-arid and semi-humid climate zones, which plays an important role on the regional ecological stability. Due to the special geographical location and natural conditions, the basin has a fragile ecological environment, and its vegetation growth is vulnerable to climatic change and human activities. The YRB is suitable to explore the mechanisms of climate on NPP because of its great variabilities on both spatial and temporal dimensions. Thus, the objective of this study was to (1) detect the spatial and temporal pattern and changing trend of NPP in the YRB from 2000 to 2019; (2) disentangle the spatial and temporal effects of climate on NPP; (3) compare the methods of EOF, SVD and traditional correlation analysis (TCA) on exploring the relationships between climatic factors and NPP.

Materials and Methods

Case Areas

The YRB is located in north of China (95°53′E-119°5′E, 32°10′N-41°50′N) with a total area of approximately 750,000 km^2, which is one of the most important basins in China and constitutes an important ecological barrier. The terrain of YRB is high in the west and low in the east (Fig. 1a). The source of YRB locates at the highest altitude of 4000 m; the altitude of the central region ranges from 1000 to 2000 m and presents a loess land form with serious soil erosion; and the eastern area is 100 m below sea level and is mainly composed of the alluvial plain of the Yellow River [25]. The geological environment is most fragile in the upper reaches of the YRB, followed by the middle reaches, and the lower reaches, and the occurrence of geological disasters presents an aggregated distribution. Under the continental monsoon circulation system, the climate in the basin is the transitional regions from semi-arid and arid to sub-humid and humid conditions. The agricultural land in the YRB is mainly dominated by grassland, farmland, and forest land (Fig. 1c).

Data Source

The MODIS product MOD17A3h6 NPP data from 2000 to 2019 was acquired from the Land Processes Distributed Active Archive Center (LP DACC), NASA (https://lpdaacsvc.cr.usgs.gov/appeears/). The data were in HDF format with 1-year temporal resolution and 500 m spatial resolution. The maximum temperature, precipitation and wind speed data were calculated from 309 meteorological stations in the YRB over the period 2000-2019. The data sourced from Climatic Data Center, National Meteorological Information Center (https://data.cma.cn/). The land coverage data set (MCD12Q1) from 2001 to 2019 across the YRB were obtained from the level-1 and atmosphere archive and distribution system (LAADS) (https://ladsweb.modaps.eosdis.nasa.gov/).

Methods and Data Processing

Spatial Distribution of Temporal Trends for NPP

The linear least-square regression method was adopted to detect the trend of the spatially averaged NPP and climate-related variables. The time series of each pixel was computed to obtain the slope coefficients of the trend line. The slope was calculated as follows:

$$\theta slope = \frac{n\times\sum_{i=1}^{n} i\times NPP_i - \sum_{i=1}^{n} i \sum_{i=1}^{n} NPP_i}{n\times\sum_{i=1}^{n} i^2 - (\sum_{i=1}^{n} i)^2} \quad (1)$$

where i is the number of the year, NPP_i represents the NPP of the i-*th* year, and slope is the temporal trend of NPP from 2000 to 2019. A slope>0 indicates an increasing trend, whereas a slope<0 indicates a decreasing trend.

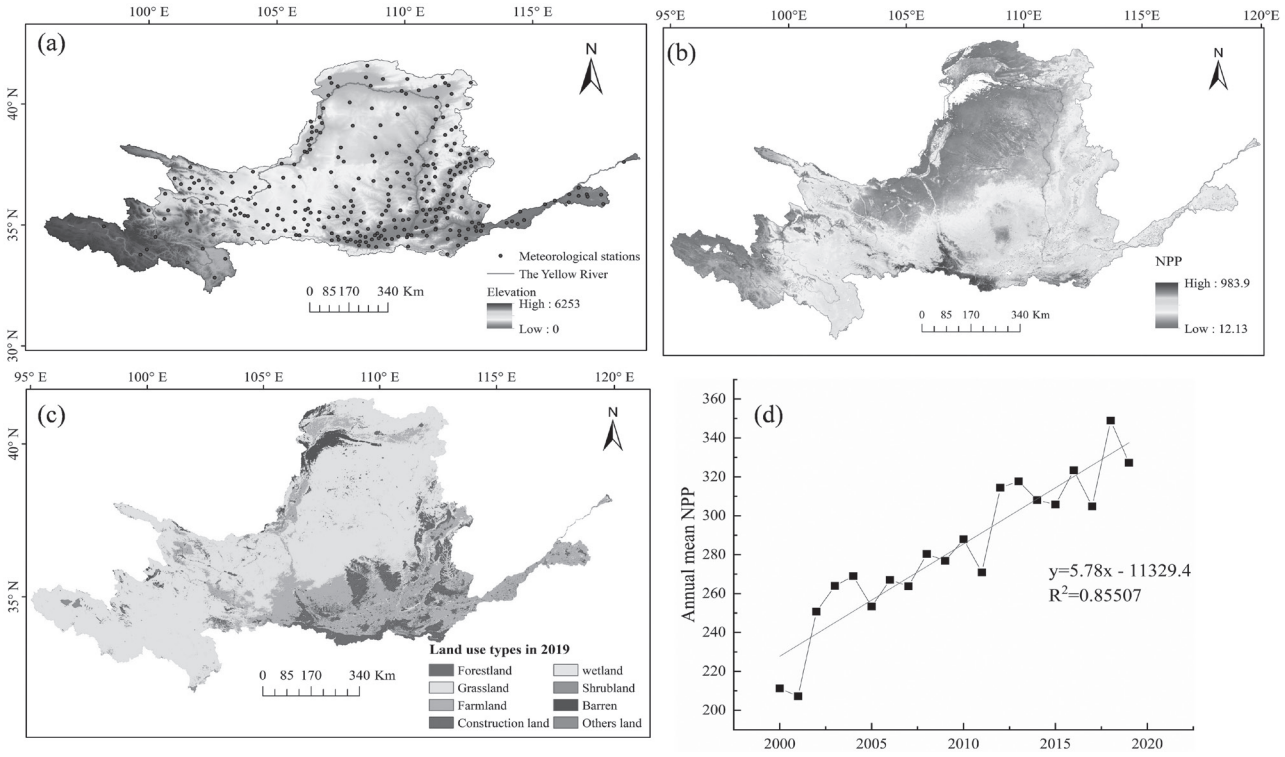

Fig. 1. a) Elevation and the distribution of selected meteorological stations; b) The spatial distribution of averaged annual NPP over 2000-2019; and c) Land use types of 2019 in the Yellow River Basin; and d) inter-annual variation of the NPP.

Empirical Orthogonal Functions (EOF) Analysis

EOF has been extensively used to analyze the spatiotemporal variability of NPP and climatic factors by decomposing the data into a set of spatial modes, which represents spatially changed pattern, and a set of corresponding time series that describes how this pattern oscillates in time [20]. Taking NPP as an example, suppose that we have removed the mean of each time series in NPP, and the NPP (F) could be represented the product of a spatial eigenvectors (C) and temporal coefficients (T):

$$F = CT \quad (2)$$

Find the covariance matrix:

$$R = F^t F = (CT)^t (CT) = C \wedge C^t \quad (3)$$

Calculate the eigenvectors and temporal coefficients of NPP:

$$RC = C \wedge \quad (4)$$

$$T = C^t F \quad (5)$$

where R is the covariance matrix, C is the eigenvectors and T is the temporal coefficient. Λ represents a diagonal matrix of the eigenvalues. The eigenvectors are ordered in accordance with the size of the eigenvalues. For example, the first mode of NPP is the eigenvector associated with the greatest eigenvalue, which represents overall variation of NPP and other patterns reflects regional difference. In general, the EOF concentrates the information of multiple variables on a few variables to explain the typical characteristics of variable field as much as possible. A detailed description of EOF can be found in previously studies [21, 26].

Singular Value Decomposition (SVD) Method

The SVD analysis can isolate coupled modes of spatial patterns and associated time series, identifying the relationship simultaneously between the NPP and climatic factors. The temporal correlation between the corresponding pairs of time series indicates the degree of coupling between NPP and climatic factors. Suppose that the mean of each time series in NPP (S) and climatic factors (P) fields has been removed, and form the covariance matrix C:

$$C = S^t P \quad (6)$$

Perform the singular value decomposition of C:

$$C = U \wedge V^t \quad (7)$$

where the singular vectors for S are the columns of U, and the singular vectors for P are the columns of V. Each pair of singular vectors is a mode of co-variability between the NPP and climate fields, and when the trends of U and V are consistent (both high or low), indicating that the NPP and climatic factors are positively correlated. Λ is the diagonal matrix.

Calculate the temporal coefficients of NPP and climatic factors:

$$A = SU \quad B = PV \quad (8)$$

where A and B represents time series of each mode, describing how each mode of variability oscillates in time. The detailed description of SVD can be found in previous studies [26].

Data Processing

The Kriging interpolation method was used to generate gridded meteorological data with the same geographic coordinate system and spatial resolution as those of the NPP data. The slope of linear least-square regression was calculated to detect the temporal variations of NPP in the YRB. TCA was employed to explore the relationship between NPP and climatic factors, and the spatial patterns and temporal series of EOF and SVD also was decomposed to identify the response of NPP to climatic changes. Finally, the results of the three methods of EOF, SVD, and TCA were compared.

Results and Discussion

The Spatiotemporal Variations of NPP

The spatial pattern of averaged NPP is presented in Fig. 1b), which decreased gradually from southeast to northwest over 2000 to 2019. Specifically, the areas with greater NPP (NPP>500) increased from 1.39% in 2000 to 13.54 % in 2015 (Table 1), and they were mainly distributed in the southeast and southern reigns. Furthermore, the areas with lower NPP (NPP<100) decreased from 18.36% in 2000 to 6.29% in 2015, where they were located in the western and northern regions. Notably, the area of the greatest NPP gradually increased from 2000 to 2015. In addition, the unchanged land types from 2001 to 2019 were extracted, and the averaged NPP showed the spatial heterogeneity in different land types: forest land had the highest mean NPP (503.07 C g/m^2), flowed by shrubland (448.51 C g/m^2), farmland (372.76 C g/m^2), wetland (316.67 C g/m^2), and grassland (229.99 C g/m^2).

The annually averaged NPP showed a significant upward trend over 2000 to 2019 in the YRB, indicating that the overall vegetation had been improved (Fig. 1d). The areas with an increasing trend accounted for 94.35% of the whole areas, and the area with a significantly greening trend was about 80.41% ($p<0.01$) (Fig. 2a and 2b). These areas mainly distributed

Table 1. The percentage of NPP in 2000, 2005, 2010, 2015.

	2000	2005	2010	2015
0-100	18.36%	12.54%	5.91%	6.29%
100-200	32.96%	27.91%	25.23%	24.84%
200-300	24.04%	21.39%	22.15%	19.98%
300-400	18.92%	23.27%	24.71%	20.79%
400-500	4.32%	10.97%	14.74%	14.56%
>500	1.39%	3.92%	7.27%	13.54%

in the central southern regions, which were mainly located in the grassland, farmland and forestland. The area percentage with decreased NPP was 5.65%, and significantly decreased areas accounted for 1.3% ($p<0.01$). Areas of significant vegetation degradation were few and scatter, which mainly located in the grassland in the western regions. The remaining degraded vegetation areas were located in the lower reaches of the YRB, which might be related to human activities.

On the whole, the area in the south had a higher NPP, because forest land and farmland were the main land types, with abundant precipitation, strong photosynthesis, and vigorous vegetation growth. In addition, the northern and western parts of the basin were located in arid areas with scarce rainfall, and the main land types were barren and grassland. The low-precipitation and serious desertification conditions made vegetation difficult to survive, resulting in lower NPP [27]. Generally, biomass and productivity varied across ecosystems, such as forest land with the highest value of NPP in the YRB, and the conversion of farmland to forest land increased the NPP in the central-south regions. Thus, the NPP was related to vegetation type and hydrothermal conditions, which was in agreement with other studies [10, 15].

The region of NPP significant improvement (66.36%) was much greater than that of degradation (0.88%). The combined effects of the implementation of ecological restoration programs and the wet-warmer climate condition promoted the increment of NPP [9, 28]. The degraded NPP were mainly distributed in the grassland of western regions, possibly caused by intensive overgrazing, which resulted in the decreasing vegetation productivity and damaged soil surface, and thus accelerating soil erosion [29]. Moreover, some studies confirmed that the frequency of extreme climate events had increased, particularly droughts, which would aggravate the regional grassland degradation [24]. Furthermore, the lower reaches of the YRB had experienced rapid urbanization and population growth, with great human disturbance on the construction land and farmland, resulting in regional degradation of NPP [30]. In recent years, a large number of ecological constructions for green space, artificial lakes, and river shelter forests have been implemented by the local government, which alleviated the pressure of urbanization on vegetation growth and limited the further expansion of the negative impact caused by human activities [31]. Therefore, it was essential to rationally allocate the green space and ecological network, which could effectively improve vegetation growth and ecological system functions [32, 33].

Correlation Analysis between NPP and Climatic Factors

The annual precipitation had a wide effect on the NPP over the Yellow River Basin, and the area with a significant positive correlation accounted for 52.65% ($p<0.05$) (Fig. 3a), which was widely distributed in the grassland of the north and northwest regions. Furthermore, the maximum temperature also had an important impact on NPP, having 20.22% ($p<0.05$) area with significantly positive correlation (Fig. 3b). These areas were mainly located in the grassland and farmland in the western and southern regions. The areas, where maximum temperature inhibits vegetation growth, were mainly distributed in the northwest regions. Moreover, positive correlations between wind speed and NPP were mainly in the centra

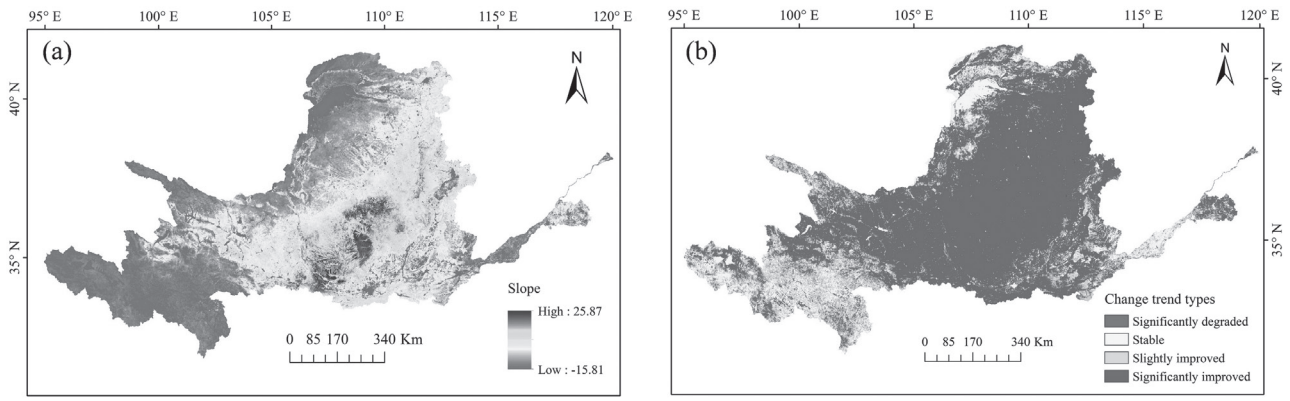

Fig. 2. a) The annual change trends in NPP; b) Four types of the overall trend.

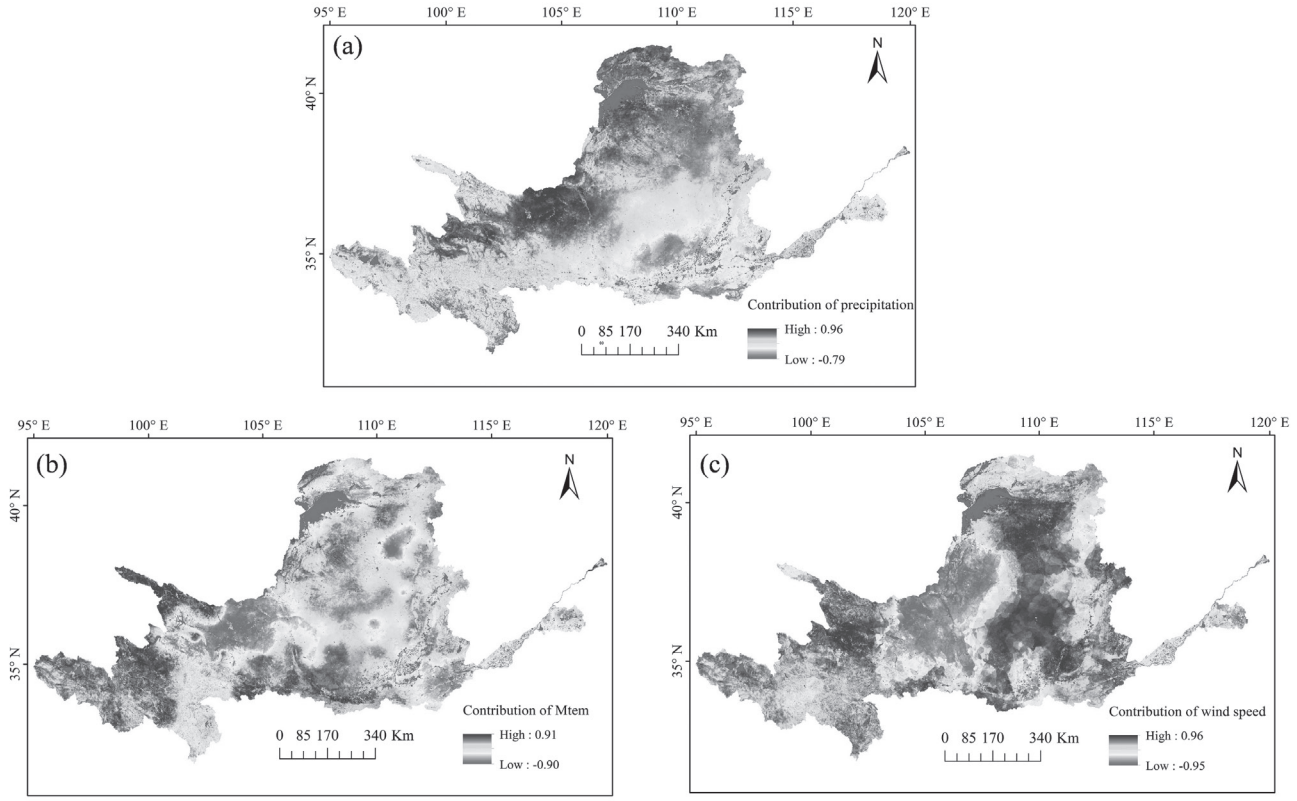

Fig. 3. The location-specific correlation relationship between NPP and climate factors. a) precipitation; b) maximum temperature, c) wind speed.

and central-northern regions, which accounted for 41.9% ($p<0.05$) (Fig. 3c). The negative correlation was mainly located in the northwest parts of the basin. Furthermore, the area significantly affected by precipitation was larger than the area affected by the wind speed and maximum temperature, indicating that precipitation was the dominant factor on NPP growth in the YRB.

In the study, the precipitation in the north of the YRB played a dominant role in NPP, which had the remarkable impact on grassland. Several studies confirmed that the contribution of each climatic factor varied in different vegetation type, which might be caused by the diversity of plant physiological structures and their adaptations to environmental variations [10, 34]. Meanwhile, some studies and this study found that precipitation had a primary factor to control the vegetation variations over arid and semiarid areas [7, 11, 20], because abundant precipitation was known to prolong the growing season into the autumn and alleviate the water stress for vegetation growth [35]. The effect of precipitation on NPP was relatively low in the south and southeast, which might be due to the fact that these regions were located in sub-humid areas, and moisture was not the main limiting factor for vegetation growth. In addition, these regions were mainly farmland and forestland, and the implementation of Yellow River Diversion Project and water conservancy measures decreased rainfall requirements for crop growth. Nevertheless, the excessive precipitation could make hypoxia of vegetation roots, and nutrient deficiency, causing the negative effect on NPP.

The maximum temperature in the western and southern of the YRB had a promoting effect on NPP, and most plants photosynthesize during daytime, and they were more sensitive to the maximum temperature [25, 36]. As the increment of maximum temperature, accelerating the thawing the frozen soil layer, and the growing season was prolonged, which was beneficial to plant growth. However, the maximum temperature exhibited inhibition for NPP in the northwest and southeast. Warmer conditions might accelerate evapotranspiration, while the higher temperature aggravated water deficiency and drought stress, especially in spring and summer, suppressing the growth of NPP [34].

The wind speed displayed a decreasing trend in the basin, which had a positive impact on NPP growth in north and central-south regions. Because of moderate wind speed could promote the gas exchange around the leaves, improve transpiration rate and increase the concentration of CO_2, accelerate the net photosynthetic rate of vegetation, thus resulted in the increment of the NPP. However, the wind speed had a significantly negative effect in northwest areas of the YRB. Excessive wind speed destroyed the leaf surface, which

reduced the transpiration and net photosynthetic rate of the plant, and weakened the photosynthesis and carbon assimilation ability of the plant, thus inhibiting the growth of NPP [37].

The Response of NPP to Climatic Factors Based on EOF

The spatial and temporal variations of NPP over the YRB were decomposed by the EOF. The spatial pattern and the associated temporal series at the first two dominant EOF modes, accounted for 54% of the total variance. The first EOF mode explained 30.6% of the total variance, which represented the mainly spatiotemporal variability of NPP (Fig. 4a). Most of the values in the first pattern were positive, indicating that the NPP change in the basin had a spatial consistency. The maximum positive value was located in the central of the basin, which implied that NPP in the area was sensitive and varied greatly. The first time series of NPP showed an increasing trend from 2000 to 2019, which indicated that the gradual improvement of NPP in the YRB, especially in the central region. The time series from 2000 to 2012 was negative, while after 2012 was positive, reaching the maximum value in 2016 (Fig. 4b). This showed that the vegetation growth status in the YRB had been greatly improved after 2012, especially in 2016.

The second EOF mode accounted for 23.4% of the total variance, which mainly represented by the NPP variation in the Lower Reach of the YRB (Fig. 4c). The maximum positive value was mainly located in the eastern part of the basin. The temporal variability of NPP showed a decreasing trend, indicating that the NPP decreased in the east. The variation range of the second time coefficient (PC2) was smaller than that of PC1, and most of the NPP PC2 were positive before 2012, and then were negative, indicating that the spatial pattern in the eastern regions had changed after 2012 (Fig. 4d).

The spatial and temporal patterns of precipitation, maximum temperature and wind speed were decomposed by EOF. The first precipitation EOF mode accounted for 27.2% of the total variance (Fig. 5a). The maximum value appeared in the northwest regions, suggesting that variation in these areas were sensitive and increased rainfall. The corresponding PC time series showed an increasing trend with strong interannual variability, and the highest value appeared in 2017 (Fig. 5c). The second precipitation EOF mode accounted for 23.3% of the total variance, which decreased from the southeast to the northwest and was similar to the spatial distribution of NPP (Fig. 5b). The temporal variability illustrated a downward trend with fluctuation and there was a peak around 2003 (Fig. 5d). The first maximum temperature EOF mode explained 87.34% of the total variance, revealing the spatial

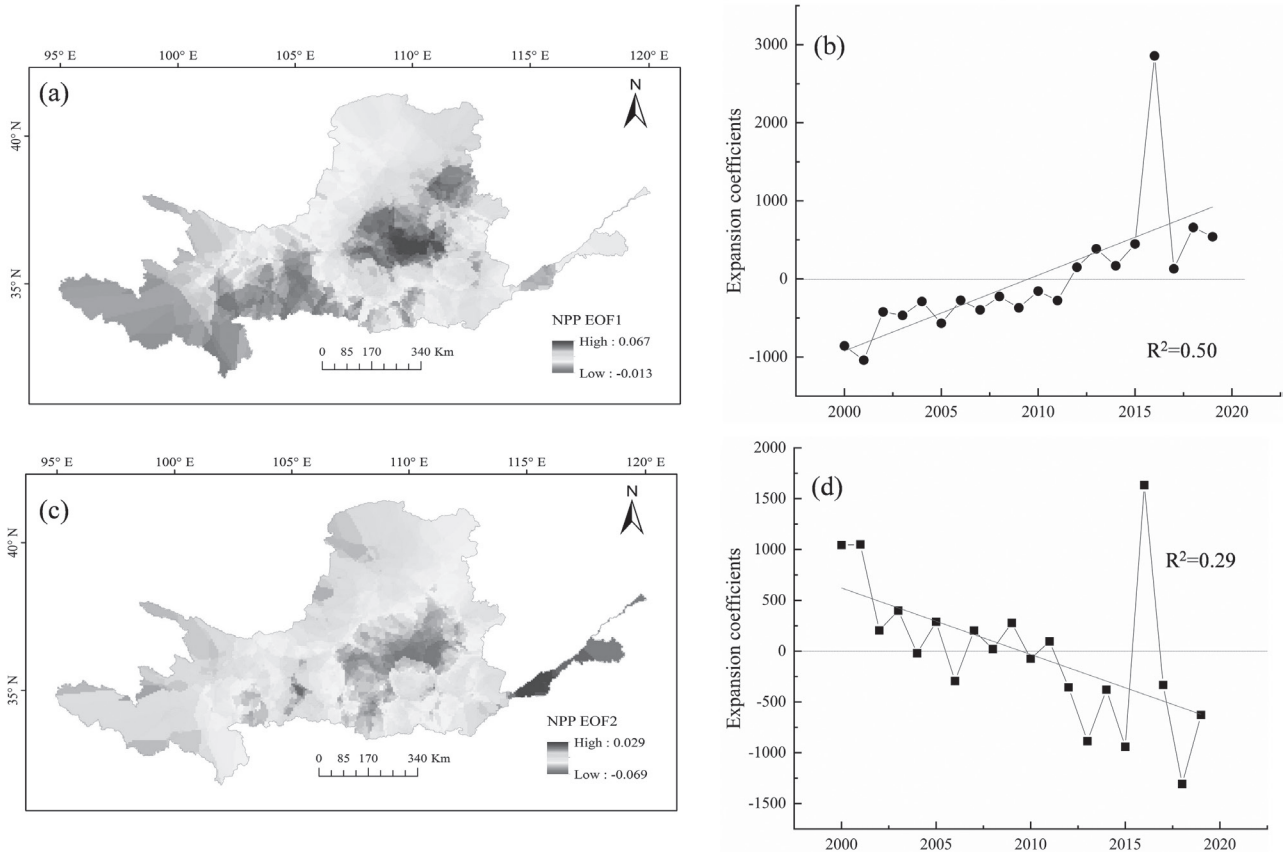

Fig. 4. a) The spatial patterns of $EOF1_{NPP}$; b) The time series of $PC1_{NPP}$; c) The spatial patterns of $EOF2_{NPP}$; (d) The time series of $PC1_{NPP}$

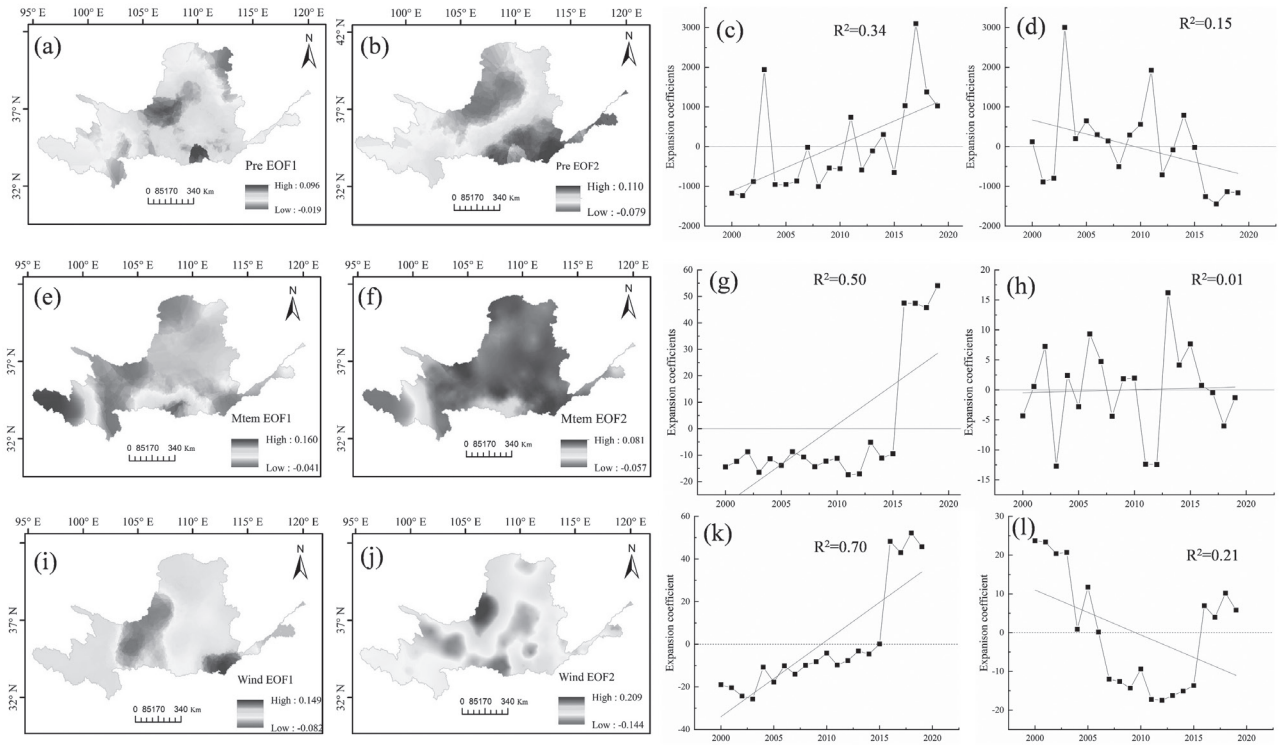

Fig. 5. The spatiotemporal variability of precipitation: a) $EOF1_{Pre}$, b) $EOF2_{Pre}$, c) $PC1_{Pre}$, d) $PC2_{Pre}$; The spatiotemporal variability of maximum temperature: e) $EOF1_{Mtem}$, f) $EOF2_{Mtem}$, g) $PC1_{Mtem}$, h) $PC2_{Mtem}$; The spatiotemporal variability of wind speed: i) $EOF1_{Wind}$, j) $EOF2_{Wind}$, k) $PC1_{Wind}$,(l) $PC2_{Wind}$.

consistency change of the maximum temperature in the study area (Fig. 5e). The maximum positive value was located in the west part of the basin, which implies that the region had stronger temperature variations. From 2000 to 2015, the temporal coefficient was negative with fluctuated. After that, it dramatically increased in 2016, and reached a maximum value, showing an upward trend (Fig. 5g). The second mode illustrated 7.75% of the total variability (Fig. 5f). The maximum value appeared in the central and the minimum appears in the west of the reign, and the time series of mode2 showed dramatic fluctuation (Fig. 5h). The first wind speed EOF explained 63.27% of the total variance (Fig. 5i). The maximum value appeared in the southeast and the minimum value appeared in the northwest. The time series showed an upward trend from 2000 to 2019, with a sharp increase in 2016 (Fig. 5k). The second EOF accounted for 21.76% of the total variance (Fig. 5j). The time coefficient showed a decreasing trend from 2000 to 2012, reached the minimum value in 2004, followed by an increasing trend (Fig. 5l).

The time series reflected how the spatial mode change with time, so the relationship between NPP and climatic factors was detected by the first time series of EOF. The correlation coefficients between $PC1_{pre}$, $PC1_{wind}$, $PC1_{mtem}$ and $PC1_{NPP}$ was 0.415, 0.645, and 0.669, respectively (Table 2), indicating that the climatic factors both were conducive to NPP growth. Furthermore, the relationship between NPP and the remaining climatic factors were strongly affected after removing maximum temperature and precipitation, respectively. This indicated that NPP was determined by the comprehensive effects of multiple climatic factors, among which maximum temperature and precipitation

Table 2. Partial correlation analysis of the time coefficient of EOF mode1.

	Factor	Precipitation	Wind speed	Maximum temperature
NPP		0.415*	0.645**	0.669**
NPP	Precipitation		0.494*	0.58**
NPP	Wind speed	0.407*		0.664**
NPP	Maximum temperature	-0.065	0.725**	

Note: * and ** represent $p<0.05$ and $p<0.01$, respectively

Table 3. The variance contribution by the first two leading modes of EOF and SVD.

Mode	Variance contribution						
	EOF_{NPP}	EOF_{PRE}	EOF_{MTEM}	EOF_{WIND}	SVD_{PRE}	SVD_{MTEM}	SVD_{WIND}
1	30.6 %	27.2%	87.34%	63.27%	30.7%	65.04%	60.66%
2	23.4 %	23.3%	7.75%	21.76%	12.42%	10.3%	14.67%
Cumulative variance	54 %	50.5%	95.09%	85.05%	43.12%	75.34%	75.33%

had great effects on ecosystem structure. Notably, wind speed had a relatively independent and remarkable effect on NPP in the YRB.

The result of spatial pattern and temporal coefficients in EOF exhibited that the ecological environment in the YRB had greatly improved, in agreement with the result of the trend analysis and other studies [38, 39]. The greatest sensitive regions of NPP were appeared in the central regions, located in the hilly and gully region of the Loess Plateau, with serious soil erosion and broken terrain, and some agricultural production activities and urbanization caused the frequently vegetation change in this area [34]. According to the decomposed spatiotemporal patterns of NPP and climatic factors, the implementation of ecological projections such as returning farmland to forest and grass and Three-North Shelter Forest Program were the main reasons for the remarkable improvement of NPP after 2012. Meanwhile, the NPP in the eastern regions had a decreasing trend, which might be related to the rapid urbanization and decreased precipitation. In addition, the maximum temperature and wind speed had a pronounced upward trend in 2016, which accelerated photosynthetic and transpiration rates, increased capacity exchange between vegetation and soil and atmosphere, and thus promoted vegetation growth in the YRB. Furthermore, the implementation of the newly revised environmental protection law in 2015 was also the cause of increased NPP. Overall, the relationship between NPP and climatic changes came from both spatial and temporal dimensions, which was controlled by the complex of ecosystem environment and the interaction between climatic factors. Wind speed played an essential role in NPP in the northwestern and southeastern regions, which were the wind erosion area and cultivation area in the YRB, respectively. In addition, this study and previous studies confirmed that the first spatial mode in EOF was similar to the trend analysis in general [20, 24, 40]. We could see that the trend analysis based on pixels mainly focused on the overall trend change of time series, which cannot describe the regional variation of a certain period in detail.

The Response of NPP to Climatic Factors Based on SVD

The SVD can separate coupled modes of variability between two fields and identify their relationship. The first paired mode of the NPP and precipitation together explained about 30.7% of the squared variance (Table 3). The spatial pattern of NPP was positive in the whole basin except the southern regions, among which the greatest sensitive regions appeared in the central and northern of the basin (Fig. 6a). The associated precipitation mode was positive in the central, northwest and west, and negative in the southern and northeastern regions (Fig. 6b). Moreover, the correlation between time series of NPP and precipitation was 0.568 ($p<0.01$), and the time series of $PC1_{NPP}$ and $PC1_{Pre}$ both exhibited an upward trend (Fig. 6c). With the increment of precipitation, NPP increased in the north, northwest and central part of the basin, decreased in the southern regions. The second paired mode explained 12.42% of the squared covariance, among which the mode of precipitation had an obviously negative center in the northwest, and a positive center in the northern regions (Fig. 6e). The positive center was located in the central-southern regions (Fig. 6d). Combining with the time series, the decreased precipitation contributed to NPP decreasing in the central-southern regions (Fig. 6f). Additionally, the correlation between the second time series was 0.673 ($p<0.01$). Overall, precipitation had a promoted effect on the growth of vegetation, and the most dominant effect of precipitation on NPP occurred in north rather than in south.

The first paired modes between NPP and maximum temperature explained 65.04% of the squared variance. The NPP mode was positive in the most of the regions (Fig. 7a). The greatest positive temperature mode was located in the west and north, and the negative temperature was in the northwest (Fig. 7b). Therefore, the increased maximum temperature contributed to the increased NPP in the west and north, and reduced NPP in the northwest. The correlation between the time series was 0.511 ($p<0.05$), implying that there was a significant relationship between NPP and maximum temperature. Furthermore, there was a great upward trend in 2016, which reflected that the highest temperature had a positive effect on NPP (Fig. 7c). The second mode of SVD illustrated 10.3% of the squared variance, and the highest temperature field showed positive value over most of the area except the western regions (Fig. 7e). The NPP field was positive in the west and northwest, while the rest of the area in the basin was negative (Fig. 7d). The correlation between the two PC time series was 0.673 ($p<0.01$) (Fig. 7f),

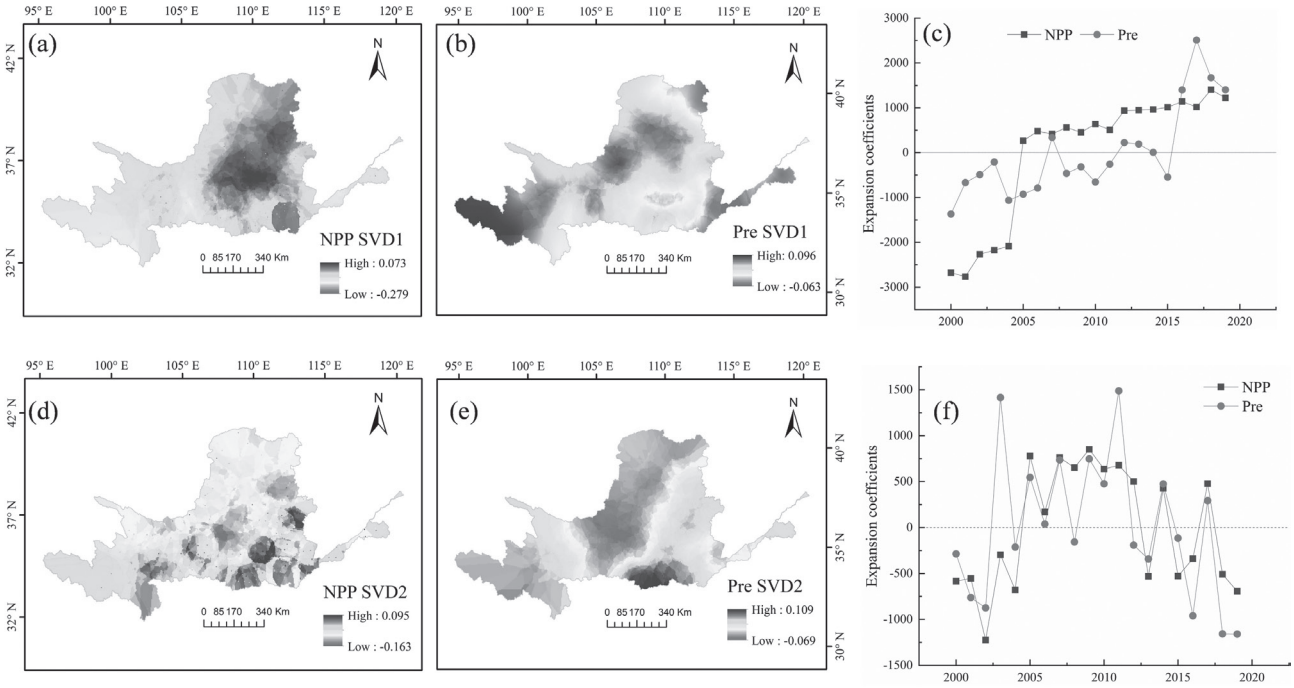

Fig. 6. The spatial patterns and time series of SVD modes between NPP and precipitation. a) $SVD1_{NPP}$; b) $SVD1_{Pre}$ c) PC1; d) $SVD2_{NPP}$; e) $SVD2_{Pre}$ f) PC2.

and the oscillation frequency of the time series was great, which indicated a strong interannual variation.

The first paired mode of NPP and wind speed explained 60.66% of the squared variance. The NPP pattern was negative across the whole basin, which indicated that the whole basin with consistent increase or decrease, and the maximum value was located in the central regions (Fig. 8a). The wind speed pattern was negative in most of the areas, while the maximum positive value appeared in the northwest (Fig. 8b).

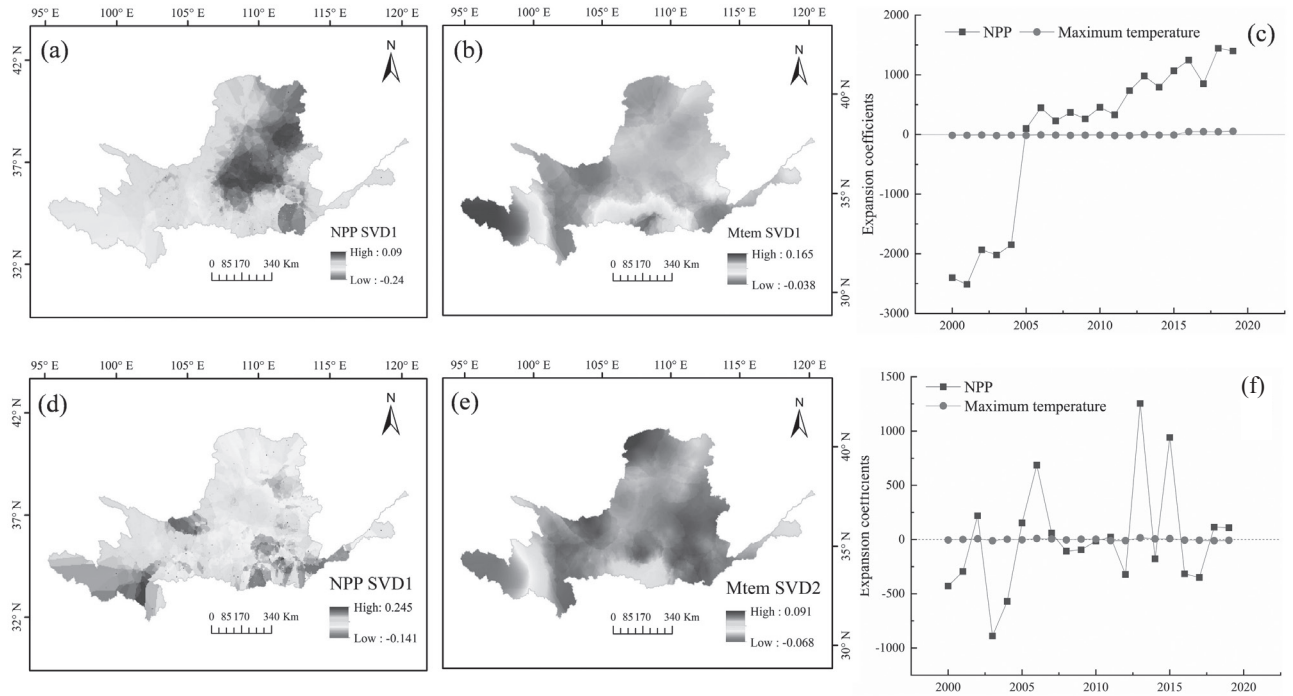

Fig. 7. The spatial patterns and time series of SVD modes between NPP and maximum temperature. a) $SVD1_{NPP}$; b) $SVD1_{Mtem}$; c) PC1; d) $SVD2_{NPP}$; e) $SVD2_{Mtem}$; f) PC2.

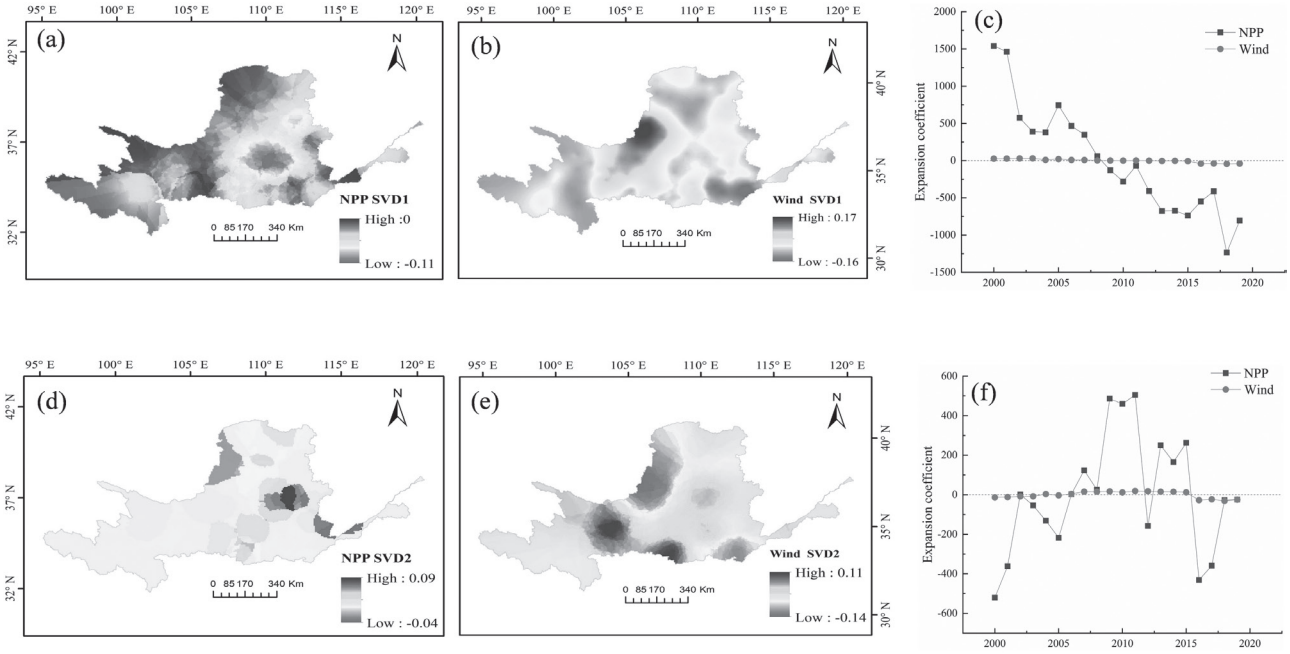

Fig. 8. The spatial patterns and time series of SVD modes between NPP and wind speed. a) $SVD1_{NPP}$; b) $SVD1_{Wind}$; c) PC1; d) $SVD2_{NPP}$; e) $SVD2_{Wind}$; f) PC2.

The correlation coefficient of the paired mode was 0.819 ($p<0.01$). Combining with the temporal series, as the wind speed increased in most areas and decreased in the northwest, NPP was getting increased in the whole basin (Fig. 8c). The second SVD mode illustrated 14.67% of the squared variance, and the correlation between the two PC time series was 0.681. The $SVD2_{NPP}$ was positive in the central regions, while the maximum value of $SVD2_{wind}$ appeared in the southwest and the minimum value was located in the northwest (Fig. 8d and e). NPP decreased in the northwest with the increment of wind 390 (Fig. 8f).

According to the coupled modes of NPP and climate variables, it was noted that the sensitivities of NPP response to climatic changes had clear spatial and temporal differences. The increment of precipitation contributed the most to NPP in the northwest and central-northern regions, which effectively compensated for the lack of soil moisture in arid and semi-arid regions, increasing the photosynthetic efficiency and the accumulation of organic dry matter. In addition, with the increment of altitude and precipitation, the photosynthesis of vegetation in western regions was mainly limited by temperature. The maximum temperature had an inhibiting effect on northwestern regions because it might contribute to stronger evaporation resulted in dry stress, limiting plant photosynthesis and growth rates. Both of precipitation and maximum temperature exhibited an increasing trend, and the wet-warm condition was beneficial to growth and restoration of vegetation [41]. Furthermore, there were differences in sensitive areas and temporal variability of NPP and climatic factors, indicating that the response of NPP to climatic changes had a time lag effect [4, 42]. It is worth noting that wind speed had an essential effect on NPP, especially in farmland in southeastern, which promoted evaporation and transpiration, and alleviated high temperature and high humidity in crop layer, increasing photosynthesis and growth of crops. In the whole, the grassland was more sensitive to changes in climatic changes than forest land and farmland, which might be related to ecosystem function, location environment, and human activities intensity. The contribution of climatic drivers to NPP was not obvious in the central and eastern of the YRB, where the impact of human activities on vegetation growth was greater than climatic changes [11, 34].

The Comparison of EOF, SVD, and TCA

There were differences in the response of NPP to climatic changes in the northeastern regions based on EOF, SVD, and TCA. The topography and geomorphology of these areas were complex, which might cause changes in regional hydrothermal conditions and soil environment, having a direct or indirect impact on NPP. TCA focused on analyzing the relationships between NPP and climatic factors of long-term series from the global scale, which might ignore and average the variation signals in regional regions. However, EOF and SVD decomposed the spatiotemporal variability of NPP and climatic factors at different scales, which could identify the variation caused by regional environmental changes. In addition, forest land and farmland were more affected by ecological engineering and human management,

and EOF and SVD could better characterize this variability at different time points. Notably, the decomposition of variability in farmland and forest land by EOF was better than SVD. Because EOF was mainly focused on single variable, and SVD could simultaneously identify variations of NPP and climatic factors, ignoring the irrelevant variation signals. Furthermore, due to the inconsistency of EOF and SVD on decomposition objects, the difference between their spatial and temporal patterns were resulted in. For example, the spatial modes of precipitation in EOF had relatively weak variability in western regions, and the correlation coefficient of the first temporal series of SVD was generally larger than EOF.

Overall, The EOF could effectively explore the spatiotemporal variability of NPP or climatic variables, and initially detect their interaction and driving effects at different scales, which was sensitive to regional variations. The SVD could identify variations between NPP and climatic factors at the same time, and the decomposed spatial and temporal patterns contained coupling relationship between variables. Compared with the EOF, the SVD analysis was a better way to reveal the response of NPP to climatic changes. Meanwhile, the TCA could directly identify the relationship between NPP and climatic factors by spatial distribution of correlation coefficients, which was simpler and more intuitive than EOF and SVD. However, TCA was sensitive to outlier points and might be limited by the number of spatial samples, and might mask some regional variations.

Conclusions

In the study, the trend analysis, TCA, EOF and SVD were used to detect the spatiotemporal variation of NPP, identify the relationship between NPP and climate factors, and the results of EOF, SVD, and TCA were compared.

(1) The annually averaged NPP decreased from southeast to northwest, and forest land had the highest value of NPP. The NPP exhibited an upward trend with fluctuations, and the areas with significantly improved vegetation were far greater than the degraded areas in the YRB, accounting for 80.41 % and 1.3%, respectively.

(2) The ecological environment of vegetation in the YRB had significantly improved since 2012 due to the implementation of ecological engineering and warm-wet climate condition, particularly in 2016. The most sensitive area of NPP was located in the central regions, where vegetation growth increased. The response of NPP to climatic factors had a time lag effect, and grassland was more sensitive to climatic changes than farmland and forestland.

(3) The contribution of precipitation on NPP was stronger than that of the maximum temperature and wind speed, and there was an interaction between climatic factors. Precipitation was a primary factor controlling the variations in NPP over water-limited regions, and the rainfall requirements for vegetation growth were related to geographic location, vegetation type, and human management practices. The maximum temperature had a positive impact on NPP in high altitude areas. Wind speed had a positive impact on NPP in most parts of basin, and a negative effect in the wind erosion region.

(4) The EOF and SVD could better identify the regional variations of NPP caused by complex topography and human activity than TCA. The characterization of variability in farmland and forest land by EOF was better than SVD. EOF mainly focused on the explanation of single variable, while SVD was better at exploring the relationship between variables. The combined method of EOF and SVD would be a good choice for the detection of vegetation variations and the relationship between vegetation growth and climatic changes.

Acknowledgments

This work has been supported financially by Natural Science foundation of Shanxi Province (201801D221103), and National Key Research and Development Program of China (2018YFE0109600).

Conflict of Interest

The authors declare no conflict of interest.

References

1. BERBEROGLU S., DONMEZ C., CILEK A. Modelling climate change impacts on regional net primary productivity in Turkey. Environmental Monitoring and Assessment, **193** (5), 242, **2021**.
2. LI S.S., LU S.H., LIU Y.P., GAO Y.H., AO Y.H. Variations and trends of terrestrial NPP and its relation to climate change in the 10 CMIP5 models. Journal of Earth System Science, **124** (2), 395, **2015**.
3. YUAN Z., WANG Y.Q., XU J.J., WU Z.G. Effects of climatic factors on the net primary productivity in the source region of Yangtze River, China. Scientific reports, **11** (1), 1376, **2021**.
4. YAN M., XUE M., ZHANG L., TIAN X., CHEN B.W., DONG Y.Q. A Decade's Change in Vegetation Productivity and Its Response to Climate Change over Northeast China. Plants, **10** (5), 821, **2021**.
5. CETIN M., ADIGUZEL F., GUNGOR S., KAYA E., SANCAR M.C. Evaluation of thermal climatic region areas in terms of building density in urban management and planning for Burdur, Turkey. Air Quality Atmosphere and Health, **12** (9), 1103, **2019**.
6. CETIN M. The effect of urban planning on urban formations determining bioclimatic comfort area's effect using satellitia imagines on air quality: a case study of Bursa city. Air Quality Atmosphere and Health, **12** (10), 1237, **2019**.

7. GE W.Y., DENG L.Q., WANG F., HAN J.Q. Quantifying the contributions of human activities and climate change to vegetation net primary productivity dynamics in China from 2001 to 2016. Science of The Total Environment, **773**, 1, **2021**.
8. VICENTE-SERRANO S.M., GOUVEIA C., CAMARERO J.J., BEGUERIA S., TRIGO R., LOPEZ-MORENO J.I., AZORIN-MOLINA C., PASHO E., LORENZO-LACRUZ J., REVUELTO J., MORAN-TEJEDA E., SANCHEZ-LORENZO A. Response of vegetation to drought time-scales across global land biomes. Proceedings of the National Academy of Sciences of the United States of America, **110** (1), 52, **2013**.
9. ZHANG H.Y., FAN J.W., CAO W., ZHONG H.P., HARRIS W., GONG G.L., ZHANG Y.X. Changes in multiple ecosystem services between 2000 and 2013 and their driving factors in the Grazing Withdrawal Program, China. Ecological Engineering, **116**, 67, **2018**.
10. GU Z.J., DUAN X.W., SHI Y.D., LI Y., PAN X. Spatiotemporal variation in vegetation coverage and its response to climatic factors in the Red River Basin, China. Ecological Indicators, **93**, 54, **2018**.
11. ZHANG W., WANG L.C., XIANG F.F., QIN W.M., JIANG W.X. Vegetation dynamics and the relations with climate change at multiple time scales in the Yangtze River and Yellow River Basin, China. Ecological Indicators, **110**, 105892, **2019**.
12. ZAREI A., CHEMURA A., GLEIXNER S., HOFF H. Evaluating the grassland NPP dynamics in response to climate change in Tanzania. Ecological Indicators, **125**, 107600, **2021**.
13. XU X., JIANG H.L., GUAN M.X., WANG L.F., HUANG Y.M., JIANG Y., WANG A.L. Vegetation responses to extreme climatic indices in coastal China from 1986 to 2015. Science of The Total Environment, **744**, 140784, **2020**.
14. LIU H.Y., JIA J.H., LIN Z.S., WANG Z.Y., GONG H.B. Relationship between net primary production and climate change in different vegetation zones based on EEMD detrending – A case study of Northwest China. Ecological Indicators, **122**, 107276, **2021**.
15. JIANG H.L., XU X., GUAN M.X., WANG L.F., HUANG Y.M., JIANG Y. Determining the contributions of climate change and human activities to vegetation dynamics in agro-pastural transitional zone of northern China from 2000 to 2015. Science of the Total Environment, **718**, 134871, **2020**.
16. WU S.H., ZHOU S.L., CHEN D.X., WEI Z.Q., DAI L., LI X.G. Determining the contributions of urbanisation and climate change to NPP variations over the last decade in the Yangtze River Delta, China. Science of The Total Environment, **472**, 397, **2014**.
17. ZHOU Y.Y., YUE D.X., LI C., MU X.L., GUO J.J. Identifying the spatial drivers of net primary productivity: A case study in the Bailong River Basin, China. Global Ecology and Conservation, **28**, e01685, **2021**.
18. WANG Z.Y., ZHONG J.L., LAN H., WANG Z.B., SHA Z.Y. Association analysis between spatiotemporal variation of net primary productivity and its driving factors in inner mongolia, china during 1994–2013. Ecological Indicators, **105**, 355, **2019**.
19. BIANCHI E., VILLALBA R., SOLARTE A. NDVI Spatio-temporal Patterns and Climatic Controls Over Northern Patagonia. Ecosystems, **23** (1), 84, **2020**.
20. HUA W.J., CHEN H.S., ZHOU L.M., XIE Z.H., QIN M.H., LI X., MA H.D., HUANG Q.H., SUN S.L. Observational Quantification of Climatic and Human Influences on Vegetation Greening in China. Remote Sensing, **9** (5), 425, **2017**.
21. CHU H.J. Spatiotemporal analysis of vegetation index after typhoons in the mountainous watershed. International Journal of Applied Earth Observation & Geoinformation, **28**, 20, **2014**.
22. PENA M.M.A., NAVARRO F.A.R. An NDVI-data harmonic analysis to study deforestation in Peru's Tahuamanu province during 2001-2011. International Journal of Remote Sensing, **37** (4), 856, **2016**.
23. LI J.C., WANG J.R., GONG B., GAN X.L., HU W.W., LIU W.L. Spatiotemporal Changes of Vegetation Cover in Response to Climate Change on the Tibetan Plateau. Acta Geologica Sinica-English Edition, **88** (3), 974, **2014**.
24. HAO L., PAN C., LIU P.L., ZHOU D.C., ZHANG L.X., XIONG Z., LIU Y.Q., SUN G. Detection of the Coupling between Vegetation Leaf Area and Climate in a Multifunctional Watershed, Northwestern China. Remote Sensing, **8** (12), 1032, **2016**.
25. MA L.Q., XIA H.M., MENG Q.M. Spatiotemporal Variability of Asymmetric Daytime and Night-Time Warming and Its Effects on Vegetation in the Yellow River Basin from 1982 to 2015. Sensors, **19** (8), 1832, **2019**.
26. BJORNSSON H., VENEGAS S.A. A Manual for EOF and SVD Analysis of Climatic Data. CCGCR Report, **97** (1), 55, **1997**.
27. ADIGUZEL F., CETIN M., KAYA E., SIMSEK M., GUNGOR S., BOZDOGANSERT E. Defining suitable areas for bioclimatic comfort for landscape planning and landscape management in Hatay, Turkey. Theoretical and Applied Climatology, **139** (3-4), 1493, **2020**.
28. ZHANG W., WANG L.C., XIANG F.F., QIN W.M., JIANG W.X. Vegetation dynamics and the relations with climate change at multiple time scales in the Yangtze River and Yellow River Basin, China. Ecological Indicators, **110**, 105892, **2020**.
29. YANG Y., WANG Z.Q., LI J.L., GANG C.C., ZHANG Y.Z., ZHANG Y., ODEH I.W., QI J.G. Comparative assessment of grassland degradation dynamics in response to climate variation and human activities in China, Mongolia, Pakistan and Uzbekistan from 2000 to 2013. Journal of Arid Environments, **135**, 164, **2016**.
30. CETIN M. Sustainability of urban coastal area management: A case study on Cide. Journal of Sustainable Forestry, **35** (7), 527, **2016**.
31. CETIN M. Using GIS analysis to assess urban green space in terms of accessibility: case study in Kutahya. International Journal of Sustainable Development and World Ecology, **22** (5), 420, **2015**.
32. BOZDOGAN SERT E., KAYA E., ADIGUZEL F., CETIN M., GUNGOR S., ZEREN CETIN I., DINC Y. Effect of the surface temperature of surface materials on thermal comfort: a case study of Iskenderun (Hatay, Turkey). Theoretical and Applied Climatology, **144** (1-2), 103, **2021**.
33. CETIN M. Climate comfort depending on different altitudes and land use in the urban areas in Kahramanmaras City. Air Quality Atmosphere and Health, **13** (8), 991, **2020**.
34. MIAO C.Y., YANG L., CHEN X.H., GAO Y. The vegetation cover dynamics (1982-2006) in different erosion regions of the Yellow River Basin, China. Land Degradation & Development, **23** (1), 62, **2012**.
35. LIU Q., FU Y.S.H., ZENG Z.Z., HUANG M.T., LI X.R., PIAO S.L. Temperature, precipitation, and insolation

effects on autumn vegetation phenology in temperate China. Global Change Biology, **22** (2), 644, **2016**.
36. PENG S.S., PIAO S.L., CIAIS P., MYNENI R.B., CHEN A.P., CHEVALLIER F., DOLMAN A.J., JANSSENS I.A., PENUELAS J., ZHANG G.X., VICCA S., WAN S.Q., WANG S.P., ZENG H. Asymmetric effects of daytime and night-time warming on Northern Hemisphere vegetation. Nature, **501** (7465), 88, **2013**.
37. GARDINER B., BERRY P., MOULIA B. Review: Wind impacts on plant growth, mechanics and damage. Plant Science, **245**, 94, **2016**.
38. TIAN F., LIU L.Z., YANG J.H., WU J.J. Vegetation greening in more than 94% of the Yellow River Basin (YRB) region in China during the 21st century caused jointly by warming and anthropogenic activities. Ecological Indicators, **125** (2), 107479, **2021**.
39. JIANG W.G., YUAN L.H., WANG W.J., CAO R., ZHANG Y.F., SHEN W.M. Spatio-temporal analysis of vegetation variation in the Yellow River Basin. Ecological Indicators, **51**, 117, **2015**.
40. PARK H.S., SOHN B.J. Recent trends in changes of vegetation over East Asia coupled with temperature and rainfall variations. Journal of Geophysical Research-Atmospheres, **115**, D14101, **2010**.
41. WANG M., FU J.E., WU Z., PANG Z. Spatiotemporal Variation of NDVI in the Vegetation Growing Season in the Source Region of the Yellow River, China. Isprs International Journal of Geo-Information, **9** (4), 282, **2020**.
42. ZHAO W., HU Z.M., GUO Q., WU G.N., CHEN R.R., LI S.G. Contributions of Climatic Factors to Interannual Variability of the Vegetation Index in Northern China Grasslands. Journal of Climate, **33** (1), 175, **2020**.